

Applications of nanophotonics to classical and quantum information technology

R. G. Beausoleil^{a,†}, D. Fattal^a, M. Fiorentino^a, C. M. Santori^a, G. Snider^a, S. M. Spillane^a, R. S. Williams^a, W. J. Munro^b, T. P. Spiller^b, J. R. Rabeau^c, S. Praver^{c,d}, F. Jelezko^e, P. Tamarat^e, J. Wrachtrup^e, and P. Hemmer^f

^aHewlett-Packard Laboratories, 1501 Page Mill Rd., Palo Alto, CA 94304, USA;

^bHewlett-Packard Laboratories, Filton Road Stoke Gifford, Bristol BS34 8QZ, UK;

^cSchool of Physics, The University of Melbourne, Melbourne, Victoria 3010, Australia;

^dCentre of Excellence for Quantum Computer Technology, School of Physics, University of Melbourne, Victoria 3010, Australia;

^ePhysikalisches Institut, Universität Stuttgart, 70550 Stuttgart, Germany;

^fElectrical & Computer Engineering Department, Texas A&M University, College Station, Texas 77843, USA

ABSTRACT

Moore's Law has set great expectations that the performance/price ratio of commercially available semiconductor devices will continue to improve exponentially at least until the end of the next decade. Although the physics of nanoscale silicon transistors alone would allow these expectations to be met, the physics of the metal wires that connect these transistors will soon place stringent limits on the performance of integrated circuits. We will describe a Si-compatible global interconnect architecture — based on chip-scale optical wavelength division multiplexing — that could precipitate an “optical Moore's Law” and allow exponential performance gains until the transistors themselves become the bottleneck. Based on similar fabrication techniques and technologies, we will also present an approach to an optically-coupled quantum information processor for computation beyond Moore's Law, encouraging the development of practical applications of quantum information technology for commercial utilization. We present recent results demonstrating coherent population trapping in single N-V diamond color centers as an important first step in this direction.

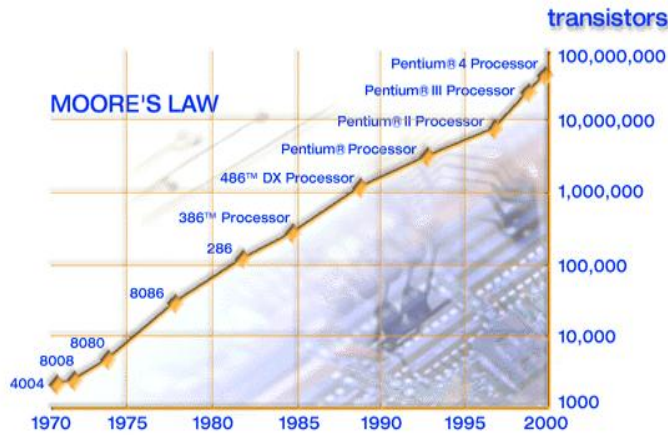
Keywords: Classical information processing, quantum information processing

1. CLASSICAL INFORMATION TECHNOLOGY

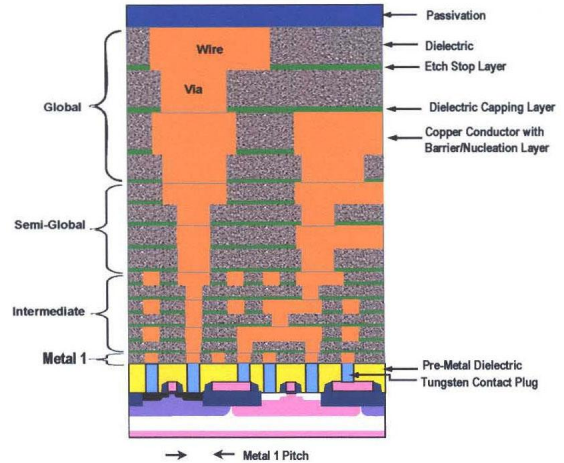
At the IEEE International Electron Devices Meeting in 1975, Gordon Moore reiterated that the number of transistors per chip N had been almost doubling annually for more than a decade. As shown in Fig. 1(a), this observation (now known — even by the general public — as “Moore's Law”) has shown few signs of relenting for over four decades. However, the information technology industry understands that the end of Moore's law as originally formulated is on the horizon, and is pushing several limits on the number of transistors per chip. Meindl has identified a five-level hierarchy of limits:¹

- Fundamental
- Material
- Device
- Circuit
- System

[†] E-mail: ray.beausoleil@hp.com



(a) Moore's Law



(b) IC cross-section

Figure 1. (a) The gift that keeps on giving: the first three decades of Moore's Law (from Intel's perspective). (b) A cross-section of a contemporary integrated circuit, showing the metal interconnect layers above the silicon.

Fundamental limits are independent of the properties of any particular material, device structure, circuit configuration, or system architecture, and are (by definition) essentially absolute and cannot be surpassed. In the same work, Meindl rigorously derived the minimum energy that must be transferred in a binary logic circuit's switching transition — the canonical computing operation — and the minimum energy that must be transferred in a single interconnect's binary transition, and found that both have precisely the value $E_s = k_B T \ln 2$, where k_B is Boltzmann's constant and T is the absolute temperature.¹

Material and semiconductor device limits fall far short of this ultimate theoretical boundary. However, if we assume that a metal oxide semiconductor field effect transistor (MOSFET) gate (input) electrode is simply a parallel plate capacitor and that at least one electron must be switched, then we can calculate the resulting transistor channel length to be approximately 10 nanometers for a dielectric gate thickness of 1 nm. Using similar arguments, Rao et al. have predicted that the ultimate speed of a transistor is proportional to the semiconductor Rydberg frequency $m^*e^4/2\epsilon_r^2\hbar^2 \approx 1$ THz, where m^* is the effective mass of the electron in the semiconductor, and ϵ_r is the relative dielectric constant.² Based on projections derived from these results and the International Technology Roadmap for Semiconductors (ITRS), a 10-nm minimum feature size could support a terascale chip — that is, a chip with 10–100 billion transistors operating at 1–10 Teraflops — sometime beyond 2020, if we can:

- demonstrate novel microfluidic methods to satisfy a terascale chip's cooling requirements;
- develop 10-nm-scale fabrication technologies that will circumvent the expected exorbitant manufacturing costs arising from optical lithographic technologies; and
- invent the necessary global interconnect technology to effectively complement 10-nm transistors.³

Although it has received relatively little attention until recently, the most problematic of these three advances is the third: even present day integrated circuits have evolved to the point where the global interconnects of the ULSI sub-micron circuits have become the most stringent limitations to performance. As shown in Fig. 1, the global interconnect now occupies over half of the metal layers of a contemporary integrated circuit.

For the past decade, the International Technology Roadmap for Semiconductors (ITRS) and its predecessor has been the blueprint that the entire world semiconductor industry uses for introducing new products (DRAM, processors and ASICs) into the market.⁴ The Roadmap provides direction for all companies that participate in the process, and most importantly points out the areas where research is urgently needed in order to overcome

Year of Production	2014	2015	2016	2017	2018	2019	2020
DRAM 1/2 Pitch (nm) (contacted)	28	25	22	20	18	16	14
MPU/ASIC Metal 1 1/2 Pitch (nm)(contacted)	28	25	22	20	18	16	14
MPU Physical Gate Length (nm)	11	10	9	8	7	6	6
Interconnect RC delay (ps) for a 1 mm minimum pitch Cu global wire, assumes no scattering and an effective ρ of 2.2 $\mu\Omega\text{-cm}$	798	896	1157	1400	1433	1814	2370
Interconnect RC delay (ps) for 1 mm Cu minimum pitch global wire, assumes width-dependent scattering and a conformal barrier of thickness specified below	1353	1601	2210	2794	2983	4064	5795
Conductor effective resistivity ($\mu\Omega\text{-cm}$) minimum pitch Cu global wiring including effect of width-dependent scattering and a conformal barrier of thickness specified below	3.73	3.93	4.20	4.39	4.58	4.93	5.38
Barrier/cladding thickness (for minimum pitch Cu global wiring) (nm) [3]	2.4	1.9	1.7	1.5	1.3	1.2	1.1
Line length (μm) where $\tau = RC$ delay (global wire at minimum pitch - no scattering)	16	14	11	10	9	7	6
Line length (μm) where 25% of switching voltage is induced on victim minimum global wire by crosstalk [4]	85	79	71	64	61	55	49
Cu thinning of maximum width global wiring due to dishing and erosion (nm), 10% \times height, 80% areal density	250	260	260	260	280	280	280
Cu thinning global wiring due to dishing (nm), 100 μm wide feature	10	9	8	7	7	6	6
Conductor effective resistivity ($\mu\Omega\text{-cm}$) Cu wiring, assumes no scattering	2.2	2.2	2.2	2.2	2.2	2.2	2.2
Interlevel metal insulator – effective dielectric constant (κ)	2.4–2.4	1.9–2.2	1.9–2.2	1.9–2.2	1.6–1.9	1.6–1.9	1.6–1.9
Interlevel metal insulator (minimum expected) – bulk dielectric constant (κ)	≤ 2.0	≤ 1.8	≤ 1.8	≤ 1.8	≤ 1.6	≤ 1.6	≤ 1.6

*Refer to Executive Summary Figure 4 for definition of metal 1 pitch

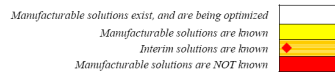


Figure 2. A long-range example from the 2005 ITRS Interconnect report. The red bricks in the table indicate that a manufacturable solution for meeting a particular requirement is *not* known.

the biggest obstacles to a particular generation of product. Nearly 100 organizations and companies worldwide participate in formulating the roadmap, which is now completely revised every other year (odd years), and significantly updated in the intervening (even) years. Beginning with the 2005 edition of the Roadmap, global interconnect has been identified as the major challenge to the the long-term growth of the semiconductor industry. This issue is illustrated in Fig. 2, which presents a long-range example from the 2005 ITRS Interconnect report. Note that the “long term” in the 2005 ITRS report begins in the year 2010, for which much of the Interconnect roadmap is red, meaning that “manufacturable solutions for the Roadmap requirements are NOT known.”

The global interconnect is responsible for conducting information over “long distances” on the chip, and to and from the chip edges. These long wires becoming the primary bottleneck for chip design and operation. The relatively slow propagation of electrical signals down the global interconnect and the relatively long distances that need to be covered are the primary limitations to the clock speed of a processor chip, and this problem is getting worse as feature sizes (e.g. wire widths) are getting smaller. Global interconnect can also consume a substantial fraction (as much as half) of the power used on a chip built using current architectures, and this problem will worsen as the wire widths sizes shrink.⁵

The problem is many-fold. First, the RC time constant of an electronic interconnect line is proportional to the square of the length of that line, since both R and C are proportional to the wire length. As the clock frequency increases, this places a severe constraint on how long global interconnect lines can be, especially for any synchronous system. Second, as the widths of the interconnect wires decrease, the RC time constant per unit length increases rapidly primarily because the effective resistivity of the copper interconnect wires rises with decreasing wire cross-section. (This increase in the effective wire resistivity noted by the ITRS is the result of the increasing importance of surface scattering as the surface to volume ratio of the wires increases.) The only known way to partially offset this increase in RC is to use an insulator with a lower dielectric constant, but the industry has been stuck with a dielectric in the range of 3.3–3.6, and has found that “the slower than projected pace of low-dielectric introduction” was one of the central issues for the ITRS. Even if the dielectric constant of the insulating layers can be reduced to 2.4, this would still only help the situation by 33%, while the problems with RC are increasing exponentially with reduced feature size. This inability to decrease the capacitance is also a major problem for dynamic power dissipation on the chip, which obeys the relation $P_{\text{dyn}} \approx CV^2f$, where

C is the capacitance of the system being charged, V is the voltage to which it is charged, and f is the charging frequency.

In 1989, Miller proposed that photonics could be used to solve the impedance mismatch problem in semiconductor chips,⁶ but for many years there has been no practical, cost-effective approach for the extraordinary level of optoelectronic integration that the global interconnect of modern ULSI integrated circuit would require. This constraint has changed dramatically within the last several years, however, as research and development in both passive and active nanophotonic devices has increased dramatically.⁷ Impressive new results on silicon photonic chips — such as demonstrations of broadband optical parametric gain near 1550 nm,⁸ and a strong quantum-confined Stark effect in germanium quantum-well structures on silicon⁹ — show that the rate of progress has not slowed. One new company, Luxtera, has combined this research with several of their own breakthroughs to push these integration concepts to the limit, and will soon offer a 40-Gbit/s DWDM CMOS optical link at a remarkable industry price point.¹⁰

This recent progress in both industry and academia has been so dramatic that a long-term R&D program to apply both time-division multiplexing (TDM) and dense wavelength-division multiplexing (DWDM) techniques to high-performance integrated circuit (IC) design has become attractive. In a typical architecture,

1. the nanocircuits are subdivided into many independent units, each with its own local multiplexing system;
2. each nanoelectronic subunit is assigned a unique frequency “fingerprint;” and
3. a two-way optical data transfer bus is provided between a central signaling system and each circuit subunit.

It is important to note that these optical data pathways can be driven in parallel, and operate at the group velocity of light in the optical substrate, providing high performance with low system complexity. In order for the promise of low power dissipation to be realized, however, the efficiency of photonic nanostructures, nanoscale photodetectors, and electro-optic modulators (i.e., performance per unit area and per unit of dissipated power) must be reduced significantly. Even more critically, the cost per Watt of optical power of modern laser sources (historically highly resistant to gigascale ULSI integration) must be reduced by at least one order of magnitude.

As daunting as these requirements seem, the end goal is extraordinarily attractive. The electronics industry has been driving the scale of device features to the de Broglie wavelength of the electron for 50 years, leading to a generalized “Moore’s Law:” the exponential improvement in information processing device performance with time. Photonic technologies have not yet seen a similar acceleration of performance improvements; in current optical information technology, the term “high level of integration” implies that functionality has been added during post-processing or packaging. Although optical IT is ultimately limited by the wavelength of light and the energy required to generate photons, photonic crystals may allow us to reach optoelectronic feature sizes as small as 1/10, and devices capable of operating at light levels of only a few photons. Ongoing research conducted by HP and sponsored by DARPA in a related technological field is already driving toward the development of novel nanoscale photonic technologies that have been manufactured using economically promising methods such as nanoimprint lithography. Therefore, this is an opportune time to investigate the integration of these techniques in an opto-electronic device that incorporates both photons and electrons used to their greatest advantage in their respective domains. In this sense, a “high level of integration” of novel photonic functional devices could occur in nanoscale monolithic fabrication rather than in post-processing, ushering in an era of “Moore’s Law” for optics.

2. QUANTUM INFORMATION TECHNOLOGY

2.1. Introduction

The search for devices that exploit quantum coherence in non-trivial fashions has rapidly become one of the major technological challenges of the twenty-first century. This search has as its goals devices ranging in complexity from single photon sources to massively entangled quantum computers. Tied to the technological imperatives are the theoretical underpinnings of a new understanding of quantum mechanics: quantum information processing

(QIP), and the quest to build new devices is closely linked to the desire to fully understand the new, and often surprising, possibilities afforded by entangled quantum systems.

For QIP applications, photon-based implementations have a privileged place. As individual quantum systems, photons are perhaps the easiest to manipulate, and without internal structure, superposition states of, for example, polarization states or modes in an interferometer, can be maintained with negligible decoherence. Hence they are ideal candidates for qubits (two-state quantum systems). Historically, one of the first suggestions for an implementation of a two-qubit gate was in an optical system, exhibiting a large lossless Kerr-type nonlinearity,¹¹ however this (and related) scheme requires a nonlinearity sufficient to impart a $\pi/2$ phase shift, for an intensity change of a single photon without any photon absorption. Whilst in principle possible, this appears out of the range of practical implementations for some time to come. Non-deterministic schemes, typified by the KLM scheme¹² present one way to realize scalable quantum computing, although the extra overhead in terms of number of photons used per gate may be undesirable.

An alternative approach is to use systems exhibiting a weak, lossless nonlinearity, and to use homodyne measurement of a *strong* probe field to effectively magnify the resultant nonlinearity, and realize a quantum non-demolition (QND) measurement of an unknown field, representing the qubit. This application (discussed below) forms the context for the present work.

Nitrogen-vacancy (N-V) centers in diamond have attracted much interest in the field of quantum information because they have long-lived electronic spin levels coupled to moderately strong optical transitions. For example, optical readout of the electronic spin of a single N-V center has been reported¹³ as well as the ability to control the coupling between spins of electrons and nuclei.¹⁴ These results have led to proposals for quantum-information applications including single photon sources,^{15–17} quantum memories and repeaters,¹⁸ quantum computation using electron spins controlled by microwave fields,¹⁹ and quantum computation based on all-optical manipulation of electron spins.²⁰ Methods of fabrication of monolithic, microstructured diamond containing N-V centers, suitable for QIP applications has been reported,²¹ and diamond as a matrix for QIP has been recently reviewed.²² Here, we investigate the feasibility of using diamond N-V centers for nonlinear optics and quantum non-demolition measurement at the single-photon level.

Nonlinear-optical devices based on EIT, as well as all-optical manipulation of electron spin, requires two ground states to be connected to a common excited state by optical transitions. However, in N-V diamond, it is not clear from the existing literature how to realize this. Recently it has been widely believed¹⁹ that the optical transitions between the 3A ground states and 3E excited states are almost perfectly spin-preserving. This is convenient for optical readout of the spin state of an N-V center, since many fluorescence cycles may be excited without changing the spin state, but this would preclude the possibility of obtaining a Λ system. To solve this problem, it has been proposed that a Λ system could be obtained by applying a particular magnetic field of approximately 0.1 T, close to an anticrossing between the $m_s = -1$ and $m_s = 0$ ground states. Close to this anticrossing, the eigenstates are linear combinations of $m_s = -1$ and $m_s = 0$ that each couple to the same pair of excited states. This technique was used by Hemmer and collaborators to demonstrate an EIT effect in N-V diamond.²³

However, we have observed coherent population trapping at zero magnetic field for ensembles nitrogen-vacancy centers in diamond under direct optical excitation.²⁴ This was measured as a reduction in photoluminescence when the detuning between two excitation lasers matched the 2.88 GHz crystal-field splitting of the color center ground states. This behavior is highly sensitive to strain, which modifies the excited states, and was unexpected following recent experiments demonstrating optical readout of single nitrogen-vacancy electron spins based on cycling transitions.¹³ These preliminary results demonstrated for the first time that three-level Lambda configurations suitable for proposed quantum information applications can be realized simultaneously for all four orientations of nitrogen-vacancy centers at zero magnetic field. In Section 2.3, we describe an extension of these techniques to demonstrations of coherent population transfer in *single* color centers, an important first step towards QIP.

2.2. Applications of EIT to Quantum Information Processing

In previous work,^{25,26} we considered a model of the nonlinear electric dipole interaction between three quantum electromagnetic radiation fields with angular frequencies ω_a , ω_b , and ω_c and a corresponding four-state atomic

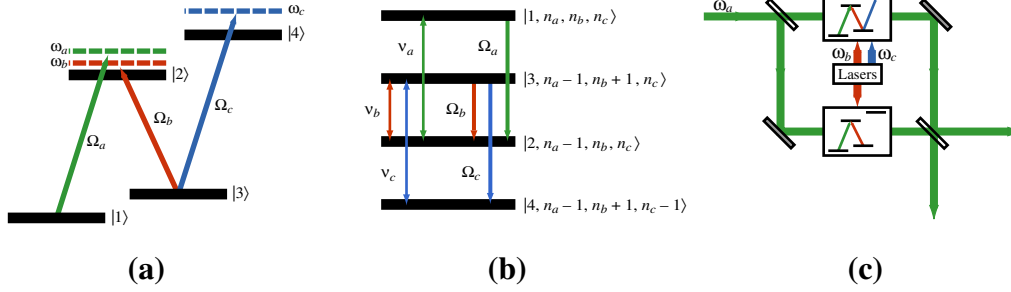


Figure 3. Electric dipole interaction between a four-state \mathcal{N} atom and a nearly resonant three-frequency electromagnetic field. (a) In the semiclassical view, two atomic states are separated by the energy $\hbar\omega_{ij}$, and coupled by a field oscillating at the frequency $\omega_k = \omega_{ij} + \nu_k$. The strength and phase of the corresponding dipole interaction is represented by the Rabi frequency $\Omega_k \propto \sqrt{n_k}$. (b) In the quantum view, the states of the atom + photons system separate into manifolds coupled internally by resonant transitions. (c) A model Mach-Zehnder interferometer illustrating an architecture for a “dual rail” quantum phase-shifter using four-state \mathcal{N} atoms. The upper arm is denoted by “1” and the lower arm by “0.”

system in the \mathcal{N} configuration, as shown in Fig. 3(a). We considered a fixed number, N , of atoms, that are stationary in a volume small compared to the optical wavelengths, and we assumed that the three frequency channels of the resonant four-state manifold of the resulting quantum system shown in Fig. 3(b) are driven by Fock states containing n_a , n_b , and n_c photons, with corresponding Rabi frequencies Ω_a , Ω_b , and Ω_c , respectively. As an example of the use of an EIT system as a phase-shifter, we incorporate the atomic system into the dual-rail Mach-Zehnder interferometer shown in Fig. 3(c). Our measurement result is a phase shift to the photon in mode a on the upper rail, conditioned on the presence of one or more photons in mode c , which represents the unknown qubit state. Mode b is used to create the necessary EIT nonlinearity in the Λ or \mathcal{N} configuration. In one arm of the interferometer, the four-state atoms are prepared using $\Omega_c \neq 0$ to provide a phase shift at the probe frequency ω_a while remaining largely transparent and dispersive. In the second arm, $\Omega_c = 0$, and the system is tuned to match the absorption and dispersion provided by the atoms in the first arm, allowing the interferometer to remain time-synchronous.

2.2.1. Single-photon QND detector

We have proposed²⁷ an implementation of the quantum non-demolition (QND) single-photon detection scheme originally described by Imoto, Haus and Yamamoto,²⁸ with the required optical nonlinearity provided by the giant Kerr effect achievable with AC Stark-shifted electromagnetically induced transparency (EIT).^{29,30} The effect of the QND measurement in turn means that signal photons are not destroyed and can be reused if required.³¹ Before we begin our detailed discussion of the EIT detection scheme, we first consider the photon number QND measurement using the cross-Kerr nonlinearity^{28,32} given by

$$H_{\text{Kerr}} = \hbar\tilde{W} a^\dagger a c^\dagger c \quad (1)$$

Here the QND signal (probe) mode has the creation and destruction operators given by a^\dagger, a (c^\dagger, c) respectively. If the signal field contains n_a photons and the probe field is in an initial coherent state with amplitude α_c , the cross-Kerr optical nonlinearity causes the combined system to evolve as

$$|\Psi(t)\rangle_{\text{out}} = e^{i\tilde{W}ta^\dagger ac^\dagger c} |n_a\rangle |\alpha_c\rangle = |n_a\rangle |\alpha_c e^{in_a \tilde{W}t}\rangle. \quad (2)$$

We observe immediately that the Fock state $|n_a\rangle$ is unaffected by the interaction, but the coherent state $|\alpha_c\rangle$ picks up a phase shift directly proportional to the number of photons n_a in the $|n_a\rangle$ state. If we measure this phase shift using a homodyne measurement (depicted schematically in Fig. 4, we can infer the number of photons in the signal mode a . The homodyne apparatus allows measurement of the quadrature operator $\hat{x}(\phi) \equiv ce^{i\phi} + c^\dagger e^{-i\phi}$, with an expected result $\langle \hat{x}(\phi) \rangle = 2\text{Re}[\alpha_c] \cos \delta + i2\text{Im}[\alpha_c] \sin \delta$, where $\delta = \phi + n_a \tilde{W}t$. For a real initial α_c , a highly efficient homodyne measurement of the momentum quadrature $Y \equiv \hat{x}(\pi/2)$ would yield the signal

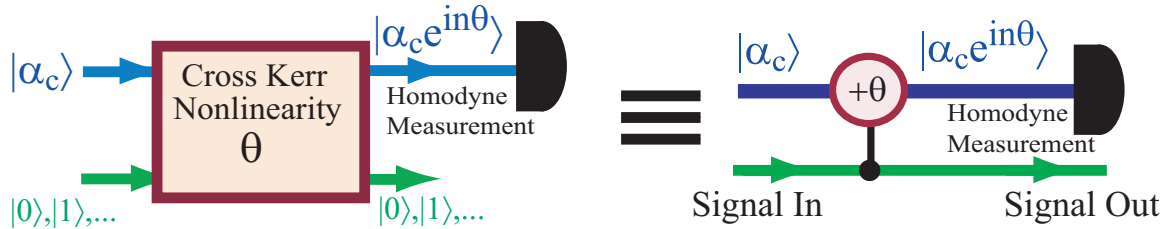


Figure 4. Schematic diagram of a photon number quantum non-demolition detector based on a cross-Kerr optical nonlinearity and a homodyne measurement.²⁸ The two inputs are a Fock state $|n_a\rangle$ (with $n_a = 0, 1, \dots$) in the signal mode a and a coherent state with real amplitude α_c in the probe mode c . The presence of photons in mode a causes a phase shift on the coherent state $|\alpha_c\rangle$ directly proportional to n_a which can be determined with a momentum quadrature measurement.

$\langle Y \rangle = 2\alpha_c \sin(n_a \tilde{W}t)$ with a variance of one, thus giving a signal-to-noise ratio of $\text{SNR}_Y = 2\alpha_c \sin(n_a \tilde{W}t)$. If the input in mode a is either the Fock state $|0\rangle$ or $|1\rangle$, the respective output states of the probe mode c are the coherent states $|\alpha_c\rangle$ or $|\alpha_c e^{i\tilde{W}t}\rangle$. Using the momentum quadrature measurement, the probability of misidentifying one of these states for one another is then $P_{\text{error}} = \frac{1}{2} \text{erfc}(\text{SNR}_Y / 2\sqrt{2})$. A signal-to-noise ratio of $\text{SNR}_Y = 4.6$ would thus give $P_{\text{error}} \sim 10^{-2}$. To achieve the necessary phase shift we require $\alpha_c \sin(\tilde{W}t) \approx 2.3$, which can be achieved in a number of ways dependent upon the range of values available for α_c and $\tilde{W}t$. For example, we could choose $\alpha_c \gg 2.3$ with $\tilde{W}t$ small and satisfy the above inequality; alternatively we could choose $\tilde{W}t = \pi/2$ with $\alpha_c = 2.3$. The particular regime chosen depends on the strength of the Kerr nonlinearity achievable in the physical system.

2.2.2. Extensions to multi-qubit quantum operations

The single-photon QND detection ideas can be applied to several photonic qubits. Basically, to perform a more “generalized” type of measurement between different photonic qubits, the homodyne measurement could be delayed. The probe beam can then interact with several cross-Kerr non-linearities, where the signal photon mode is different in each interaction case. The probe beam measurement can then be made after all these interactions and—very importantly—be made in a collective way that could condition onto interesting two-photon states.³³ For example, a non-destructive detection can be made that distinguishes superpositions and mixtures of the states $|HH\rangle$ and $|VV\rangle$ from $|HV\rangle$ and $|VH\rangle$. The key here is that it is possible to arrange no net phase shift on the $|HV\rangle$ and $|VH\rangle$ terms while having a phase shift on the $|HH\rangle$ and $|VV\rangle$ terms. We call this generalization a *two-qubit polarization parity QND gate*.

The idea of amplifying a weak optical Kerr nonlinearity using homodyne detection and feed-forward can be extended beyond quantum nondemolition and parity detection.^{34,35} For example, using the two-photon parity gate as a primitive, a symmetry analyzer for nondestructive Bell-state measurement³³ and a CNOT gate³⁶ can (in principle) be constructed. It is not clear yet whether the required X homodyne measurement can be performed, but — by displacing the coherent probe state to the vacuum³⁷ — it is possible that QND may be used instead. Again we note, that combined with the fact that single qubit operations are easily performed with polarization optics in a photonic implementation to extremely high fidelity, the presence of any non-trivial coupling is sufficient for universal quantum computation.

2.3. Coherent Population Trapping in Nitrogen-Vacancy Color Centers

Using optical laser fields to excite and manipulate spin coherences in solids has numerous potential applications in quantum computing. An important advantage of optical manipulation over direct microwave excitation of the spin transitions is high spatial resolution, which is important for selective addressing of individual qubits.²⁰ It should be possible to use optical Raman interactions to generate coherent superpositions of ground-state spin sublevels while maintaining long spin coherence lifetimes using techniques already demonstrated with trapped ions.³⁸ All-optical spin manipulation and coherent population trapping have the same requirement: a Λ system

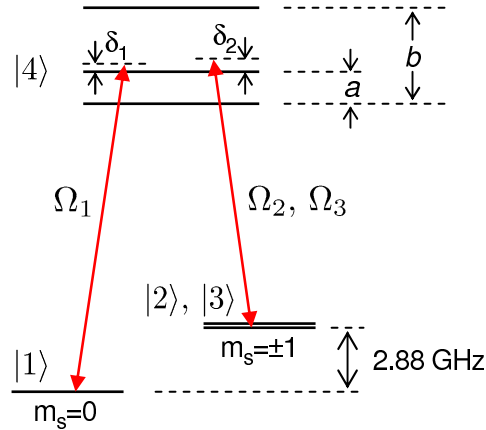


Figure 5. Schematic energy level diagram of a strained NV center.

consisting of an excited state coupled by optical transitions to two ground states, which has now been obtained in a variety of solids. For example, extremely long storage times and room-temperature CPT have been achieved in Pr:YSO³⁹ and ruby,⁴⁰ respectively, but the oscillator strengths in these materials seem much too small for experiments with single impurities. In semiconductor systems the oscillator strength can exceed unity, and in single charged quantum dots optical pumping⁴¹ and initialization of a coherent superposition of spin states⁴² have recently been reported, representing a promising step toward all-optical spin control. However, in quantum dots as well as shallow donors⁴³ the spin coherence is limited by inhomogeneous broadening of the g -factor and hyperfine interaction with a bath of randomly oriented nuclear spins.

As mentioned previously, nitrogen-vacancy (NV) defects in diamond can have extremely long-lived spin coherence because the lattice is composed primarily of ¹²C, which has zero nuclear spin. Composed of a substitutional nitrogen next to a carbon vacancy, the NV center has been studied extensively, with recent emphasis on potential applications in quantum information processing. For the negatively-charged NV center, the ground states, shown in Fig. 5, consist of a spin triplet split by the crystal field into an $m_s = 0$ level and a degenerate pair of $m_s = \pm 1$ levels 2.88 GHz higher in energy.⁴⁴ These levels are connected to excited states by optical transitions of moderate strength, with a total oscillator strength of approximately 0.2, or 0.006 for the zero-phonon line alone. By exciting a cycling transition between the $m_s = 0$ ground state and a particular excited state, readout of single spins¹³ and optically-detected electron spin resonance in a single NV center⁴⁵ have been demonstrated.

For all-optical spin manipulation it is essential for an excited state to couple to multiple ground states, and it is not clear in the existing literature how best to realize this configuration since the excited-state structure remains uncertain. Spectral-hole-burning studies on large ensembles indicate three excited levels which sometimes couple to multiple ground sublevels,^{24, 46, 47} while recent work on single NV centers suggests only parallel, spin-preserving transitions at zero magnetic field. A key finding of our recent low-temperature spectroscopy on single NV centers, to be explained in detail elsewhere,⁴⁸ is that there are roughly two types of NV centers which could be termed “bright” and “dark.” The bright centers can be observed with a single excitation laser, while the dark centers are visible only when two optical frequencies simultaneously excite the $m_s = 0$ and $m_s = \pm 1$ ground states to avoid the suppression of fluorescence by cross-relaxation. The dark centers have spin-nonpreserving transitions that are allowed, making them suitable for the work described here. Their relative proportion, depending on factors which reduce the symmetry of the NV centers, can be controlled by application of a strain field.²⁴ The level diagram in Fig. 5 is appropriate for the strained case, showing a set of three excited states, with another set of three levels at higher energy also predicted.^{49, 50}

In our experiments, to find a suitable NV center, the laser frequency was scanned while a modulator produced sidebands at ± 2.90 GHz, slightly off of resonance from the ground-state splitting, with each sideband approximately 50% as intense as the fundamental component. To observe coherent population trapping, the laser frequency is fixed on one of the two lines, and the modulation frequency is scanned across 2.88 GHz. The scans

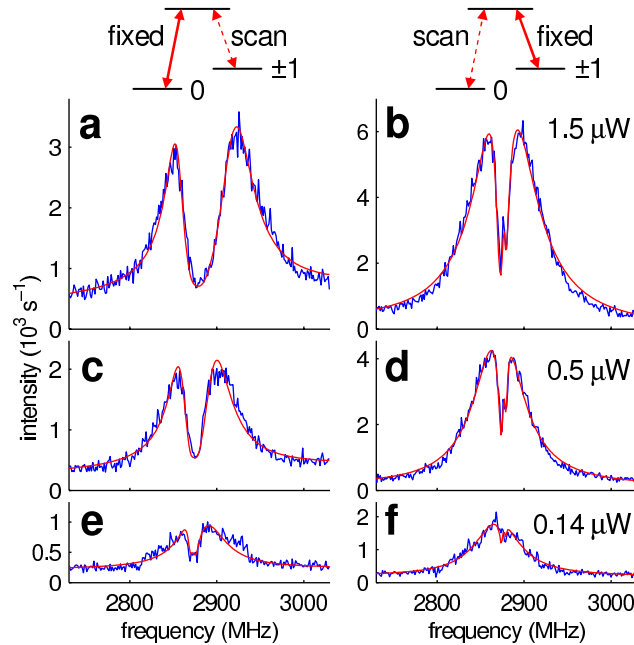


Figure 6. Measured and fitted modulation frequency scans. For **a,c,e**, laser fixed on $m_s = 0$ transition; for **b,d,f** laser fixed on $m_s = \pm 1$ transition. Excitation powers: **a,b**: $1.5 \mu\text{W}$; **c,d**: $0.5 \mu\text{W}$; **e,f**: $0.14 \mu\text{W}$.

must be performed quickly (10 Hz) to avoid photo-induced spectral jumps during the scans. Summing many of these scans together reveals a broad peak around 2.88 GHz with the characteristic dip within it representing coherent population trapping. In the summed data we see a dip that extends almost completely down to the background level, suggesting a large degree of spin coherence on two-photon resonance.

We performed a series of measurements under varied excitation conditions on an NV center with excited-state parameters $a = 0.31$ GHz and $b = 0.94$ GHz (see Fig. 5), using the middle excited state. For the graphs on the left side of Fig. 6, the laser was on resonance with the $m_s = 0$ transition while a weak modulation sideband (about 2% relative power) was scanned across the $m_s = \pm 1$ transitions, and thus the shape of the fluorescence dip gives information mainly about the $m_s = 0$ transition. For the graphs on the right, the roles of the laser and sideband were reversed, giving information about the $m_s = \pm 1$ transitions. Results from several excitation powers are shown along with model fits. From the fits we can estimate the relative transition strengths of the transitions for equal excitation power: $\Omega_2^2/\Omega_1^2 = 0.14$ and $\Omega_3^2/\Omega_1^2 = 0.05$. Thus all ground states are coupled to the middle excited state by a measurable amount. The $m_s = \pm 1$ splitting of 5 MHz visible in the graphs on the right could be due either to strain or to a background magnetic field. We estimate a ground-state decoherence rate 1.2 MHz. Analysis of the fitted density matrix close to two-photon resonance in Fig. 6a shows a nearly equal statistical mixture of the two dark states. The ground-state coherences are approximately 99% and 90%, respectively, of the maximum possible for such a mixture.

These results demonstrate steady-state formation of coherent superpositions of spin states with probability amplitudes directly tunable through the laser and sideband amplitudes. Thus all-optical coherent control of the spin state of a single NV center is possible. This capability could already be useful in repeater schemes¹⁸ where efficient coupling between a photonic qubit and the spin of the NV center is not critical. To fully realize the potential of diamond NV centers for photonic quantum information processing it will be necessary to couple them efficiently to nanophotonic cavities and waveguides. This would enhance the modest oscillator strength of the zero-phonon line and improve the extraction of the emitted photons. Then, schemes for efficient interconversion between photonic and spin qubits could be realized,⁵¹ and photons could serve as a communications bus between spatially separated spin qubits. Progress has been made toward fabrication of the necessary structures out of diamond⁵² without sacrificing the material quality. We note also that in existing microdisk resonators, for

example, a realistic quality factor of $Q = 10^6$ and a mode volume of $V = 100(\lambda/n)^3$ would be enough for efficient single-mode emission from the zero-phonon line.

Acknowledgments

We are grateful to Eli Yablonovitch for ongoing illuminating discussions. The work on N-V diamond performed at HP Laboratories in Palo Alto has been supported by DARPA and the Air Force Office of Scientific Research through AFOSR contract no. FA9550-05-C-0017. The work of the Stuttgart group was supported by DFG (project SFB/TR 21), EU (Integrated Project Qubit Applications QAP funded by the IST directorate as Contract Number 015848) and 'Landesstiftung B-W' (project 'Atomoptik'). Supported by DARPA QuIST under AFOSR contract number C02-00060. Ph. T. acknowledges the Alexander von Humboldt Foundation for a research fellowship.

REFERENCES

1. J. D. Meindl and J. A. Davis, "The Fundamental Limit on Binary Switching Energy for Terascale Integration," *IEEE J. Solid State Circuits* **35**, 1515 (2000).
2. D. S. Rao, T. Szkopek, H. W. Jiang, and E. Yablonovitch, "What is the Fastest Speed at which a Single Electron Can Be Detected?" <http://arxiv.org/abs/quant-ph/0507224>.
3. J. D. Meindl, "Beyond Moore's Law: The Interconnect Era," *Comp. Sci. Eng.*, January/February 2003, pp. 20-24.
4. The 2005 edition of the International Technology Roadmap for Semiconductors can be found at <http://www.itrs.net/Links/2005ITRS/Home2005.htm>.
5. D. A. B. Miller and H. M. Ozaktas, "Limit to the Bit-Rate Capacity of Electronic Interconnects from the Aspect Ratio of the System Architecture," *J. Parallel and Distributed Computing* **41**, 42–52 (1997).
6. D. A. B. Miller, "Optics for low-energy communication inside digital processors: quantum detectors, sources, and modulators as efficient impedance converters," *Opt. Lett.* **14**, 146–148, (1989).
7. M. Lipson, "Guiding, Modulating and Emitting Light on Silicon — Challenges and Opportunities," *IEEE J. Lightwave Technol.* **23**, 4222–4238 (2005).
8. M. A. Foster, A. C. Turner, J. E. Sharping, B. S. Schmidt, M. Lipson, and A. L. Gaeta, "Broad-band optical parametric gain on a silicon photonic chip," *Nature* **441**, 960–963 (2006).
9. Y.-H. Kuo, Y. K. Lee, Y. Ge, S. Ren, J. E. Roth, T. I. Kamins, D. A. B. Miller, and J. S. Harris, "Strong quantum-confined Stark effect in germanium quantum-well structures on silicon," *Nature* **437**, 1334–1336 (2005).
10. See <http://www.luxtera.com/>.
11. G. J. Milburn, "Quantum optical Fredkin gate" *Phys. Rev. Lett.*, **62**, 2124–2127, 1987.
12. E. Knill, L. Laflamme, and G. J. Milburn, "A scheme for efficient quantum computation with linear optics" *Nature (London)* **409**, 46–52, 2001.
13. F. Jelezko, I. Popa, A. Gruber, C. Tietz, J. Wrachtrup, A. Nizovtsev and S. Kilin, "Single spin states in a defect center resolved by optical spectroscopy," *Appl. Phys. Lett.* **81**, pp. 2160–2162 (2002).
14. E. A. Wilson, N. B. Manson and C. Wei, "Perturbing an electromagnetic induced transparency within an inhomogeneously broadened transition," *Phys. Rev. A* **67**, pp. 023812–1–10 (2003).
15. A. Beveratos, S. Kühn, R. Brouri, T. Gacoin, J-P Poizat, and P. Grangier P, "Room temperature stable single-photon source", *European Physical Journal D* **18**, 191, 2002.
16. J. R. Rabeau, S. T. Huntington, A. D. Greentree, and S. Prawer, "Diamond chemical vapour deposition on optical fibres for fluorescence waveguiding", *Appl. Phys. Lett.* **86**, 134104, 2005.
17. A. D. Greentree, J. Salzman, S. Prawer, and L. C. L. Hollenberg, "Quantum gate for Q switching in monolithic photonic bandgap cavities containing two-level atoms", to appear in *Phys. Rev. A*, quant-ph/0511107.
18. L. Childress, J. M. Taylor, A. S. Sorensen and M. D. Lukin, "Fault-tolerant quantum repeaters with minimal physical resources and implementations based on single-photon emitters," *Phys. Rev. A* **72**, pp. 052330–1–16 (2005).

19. A. P. Nizovtsev, S. Ya. Kilin, F. Jelezko, T. Gaebel, I. Popa, A. Gruber and J. Wrachtrup, "A quantum computer based on NV centers in diamond: optically detected nutations of single electron and nuclear spins," *Opt. Spectrosc.* **99**, pp. 233–244 (2005).
20. M. S. Shahriar, P. R. Hemmer, S. Lloyd, P. S. Bhatia, and A. E. Craig, "Solid-state quantum computing using spectral holes," *Phys. Rev. A* **66**, 032301 (2002).
21. P. Olivero, S. Rubanov, P. Reichart, B. Gibson, S. Huntington, J. Rabeau, A. D. Greentree, J. Salzman, D. Moore, D. N. Jamieson, S. Prawer, "Ion Beam Assisted Lift-Off Technique for Three-Dimensional Micromachining of Free Standing Single-Crystal Diamond", *Advanced Materials*, **17**, 2427-2430, 2005.
22. A. D. Greentree, P. Olivero, M. Draganski, E. Trajkov, J. R. Rabeau, P. Reichart, B. C. Gibson, S. Rubanov, S. T. Huntington, D. N. Jamieson, and S. Prawer, "Critical components for diamond-based quantum coherent devices", preprint.
23. P. R. Hemmer, A. V. Turukhin, M. S. Shahriar and J. A. Musser, "Raman-excited spin coherences in nitrogen-vacancy color centers in diamond," *Opt. Lett.* **26**, pp. 361–363 (2001).
24. C. Santori, D. Fattal, S. M. Spillane, M. Fiorentino, R. G. Beausoleil, A. D. Greentree, P. Olivero, M. Draganski, J. R. Rabeau, P. Reichart, B. C. Gibson, S. Rubanov, D. N. Jamieson, and S. Prawer, "Coherent Population Trapping in Diamond N-V Centers at Zero Magnetic Field," accepted for publication in Optics Express; preprint: <http://arxiv.org/abs/cond-mat/0602573>.
25. R. G. Beausoleil, W. J. Munro, and T. P. Spiller, "Applications of coherent population transfer to quantum information processing," *J. Mod. Opt.* **51**, pp. 1159–1601, 2004.
26. R. G. Beausoleil, W. J. Munro, D. A. Rodrigues, and T. P. Spiller, "Applications of electromagnetically induced transparency to quantum information processing," *J. Mod. Opt.* **51**, pp. 2441–2447, 2004.
27. W. J. Munro, K. Nemoto, R. G. Beausoleil, and T. P. Spiller, "High-efficiency quantum nondemolition single-photon-number-resolving detector," *Phys. Rev. A* **71**, p. 033819, 2005.
28. N. Imoto, H. A. Haus, and Y. Yamamoto, "Quantum nondemolition measurement of the photon number via the optical kerr effect," *Phys. Rev. A* **32**, pp. 2287–2292, 1985.
29. S. E. Harris, J. E. Field, and A. Imamoglu, "Nonlinear optical processes using electromagnetically induced transparency", *Phys. Rev. Lett.* **64**, 1107-1110, 1990.
30. H. Schmidt and A. Imamoglu, "Giant kerr nonlinearities obtained by electromagnetically induced transparency," *Opt. Lett.* **21**, pp. 1936–1938, 1996.
31. P. Grangier, J. A. Levenson, and J.-P. Poizat, "Quantum non-demolition measurements in optics," *Nature* **396**, pp. 537–542, 1998.
32. J. C. Howell and J. A. Yeazell, "Nondestructive single-photon trigger," *Phys. Rev. A* **62**, p. 032311, 2000.
33. S. D. Barrett, P. Kok, K. Nemoto, R. G. Beausoleil, W. J. Munro, and T. P. Spiller, "Symmetry analyzer for nondestructive Bell-state detection using weak nonlinearities," *Phys. Rev. A* **71**, p. 060302, 2005.
34. W. J. Munro, K. Nemoto, T. P. Spiller, S. D. Barrett, P. Kok, and R. G. Beausoleil, "Efficient optical quantum information processing," *J. Opt. B: Quant. Semiclass. Opt.*, **7**, pp. S135–S140 (2005).
35. W. J. Munro, K. Nemoto, and T. P. Spiller, "Weak nonlinearities: a new route to optical quantum computation," *New J. Phys.*, **7**, pp. 137–148 (2005).
36. K. Nemoto and W. J. Munro, "Nearly Deterministic Linear Optical Controlled-NOT Gate," *Phys. Rev. Lett.* **93**, p. 250502, 2004.
37. T. P. Spiller, K. Nemoto, S. L. Braunstein, W. J. Munro, P. van Loock, and G. J. Milburn, "Quantum Computation by Communication," *arXiv:quant-ph/0509202*, 2005.
38. D. Leibfried, R. Blatt, C. Monroe, and D. Wineland, "Quantum dynamics of single trapped ions," *Rev. Mod. Phys.* **75**, 281–324 (2003).
39. J. J. Longdell, E. Fraval, M. J. Sellars, and N. B. Manson, "Stopped light with storage times greater than one second using electromagnetically induced transparency in a solid," *Phys. Rev. Lett.* **95**, 063601 (2005).
40. R. Kolesov, "Coherent population trapping in a crystalline solid at room temperature," *Phys. Rev. A* **72**, 051801 (2005).
41. M. Atature, J. Dreiser, A. Badolato, A. Hoge, K. Karrai, and A. Imamoglu, "Quantum-dot spin-state preparation with near-unity fidelity," *Science* **312**, 551–553 (2006).

42. M. V. G. Dutt, J. Cheng, B. Li, X. Xu, X. Li, P. R. Berman, D. G. Steel, A. S. Bracker, D. Gammon, S. E. Economou, R.-B. Liu, and L. J. Sham, "Stimulated and spontaneous optical generation of electron spin coherence in charged GaAs quantum dots," *Phys. Rev. Lett.* **94**, 227403 (2005).
43. K. C. Fu, C. Santori, C. Stanley, M. C. Holland, and Y. Yamamoto, "Coherent population trapping of electron spins in a high-purity n-type GaAs semiconductor," *Phys. Rev. Lett.* **95**, 187405 (2005).
44. E. van Oort, N. B. Manson and M. Glasbeek, "Optically detected spin coherence of the diamond N-V centre in its triplet ground state," *J. Phys. C.* **21**, 4385-4391 (1998).
45. F. Jelezko, T. Gaebel, I. Popa, A. Gruber, and J. Wrachtrup, "Observation of coherent oscillations in a single electron spin," *Phys. Rev. Lett.* **92**, 076401 (2004).
46. N. R. S. Reddy, N. B. Manson, and E. R. Krausz, "Two-laser spectral hole burning in a colour centre in diamond," *J. Lumin.* **38**, 46-47 (1987).
47. N. B. Manson and C. Wei, "Transient hole burning in N-V center in diamond," *J. Lumin.* **58**, 158-160 (1994).
48. *To be published.*
49. J. P. D. Martin, "Fine structure of excited 3E state in nitrogen-vacancy centre in diamond" *J. Lumin.* **81**, 237-247 (1999).
50. N. B. Manson, J. P. Harrison, and M.J. Sellars, "The nitrogen-vacancy center in diamond re-visited," *preprint*: <http://arxiv.org/abs/cond-mat/0601360>.
51. J. I. Cirac, P. Zoller, H. J. Kimble, and H. Mabuchi "Quantum state transfer and entanglement distribution among distant nodes," *Phys. Rev. Lett.* **78**, 3221-3224 (1997).
52. P. Olivero, S. Rubanov, P. Reichart, B. Gibson, S. Huntington, J. Rabeau, A. D. Greentree, J. Salzman, D. Moore, D. N. Jamieson, and S. Prawer, "Ion beam assisted lift-off technique for three-dimensional micromachining of free standing single-crystal diamond," *Advanced Materials* **17**, 2427-2430 (2005).